THE JOURNAL OF BIOLOGICAL CHEMISTRY VOL. 281, NO. 52, pp. 40114–40123, December 29, 2006

PAT1a Modulates Intracellular Transport and Processing of Amyloid Precursor Protein (APP), APLP1, and APLP2*[S]

Received for publication, June 6, 2006, and in revised form, August 31, 2006 Published, JBC Papers in Press, October 18, 2006, DOI 10.1074/jbc.M605407200

Yung-Hui Kuan[‡1], Tomas Gruebl[‡1], Peter Soba[‡2], Simone Eggert[‡3], Iva Nesic[‡4], Simone Back[‡], Joachim Kirsch[§], Konrad Beyreuther[‡], and Stefan Kins[‡5]

From the [‡]Zentrum für Molekulare Biologie (ZMBH) and the [§]Department of Anatomy and Cell Biology, University of Heidelberg, D-69120 Heidelberg, Germany

Understanding the intracellular transport of the β-amyloid precursor protein (APP) is a major key to elucidate the regulation of APP processing and thus β-amyloid peptide generation in Alzheimer disease pathogenesis. APP and its two paralogues, APLP1 and APLP2 (APLPs), are processed in a very similar manner by the same protease activities. A putative candidate involved in APP transport is protein interacting with APP tail 1 (PAT1), which was reported to interact with the APP intracellular domain. We show that PAT1a, which is 99.0% identical to PAT1, binds to APP, APLP1, and APLP2 *in vivo* and describe their co-localization in trans-Golgi network vesicles or endosomes in primary neurons. We further demonstrate a direct interaction of PAT1a with the basolateral sorting signal of APP/APLPs. Moreover, we provide evidence for a direct role of PAT1a in APP/APLP transport as overexpression or RNA interference-mediated knockdown of PAT1a modulates APP/APLPs levels at the cell surface. Finally, we show that PAT1a promotes APP/APLPs processing, resulting in increased secretion of β-amyloid peptide. Taken together, our data establish PAT1a as a functional link between APP/APLPs transport and their processing.

Amyloid plaques, the major hallmark of Alzheimer disease, are mainly composed of the β-amyloid peptide (Aβ),[6] which is proteolytically derived from the β-amyloid precursor protein (APP) (1). APP belongs to a protein family with two mammalian paralogues, the β-amyloid precursor-like proteins (APLP) 1 and 2 (2–5). APP/APLPs share highly conserved protein domain organization (6), form homo- and heterotypic interactions (7), and are proteolytically processed in a similar manner (8). The extracellular domain of APP/APLPs can be cleaved by α-secretases or, alternatively, by the β-secretase β-site APP cleaving enzyme 1 (BACE 1) (8–12). The resulting membrane-retained C-terminal fragments (CTFs) are subsequently processed by cleavage within the transmembrane domain by the γ-secretase complex (13, 14). Consecutive β- and γ-cleavage of APP/APLPs results in the release of Aβ/Aβ-like peptides, whereas α- and γ-cleavage generate p3/p3-like fragments, respectively. Concomitantly, both processing pathways liberate the corresponding intracellular domains (ICDs) (8, 15, 16). A function in nuclear signaling was proposed for the APP/APLP ICDs (16–18), suggesting that processing of APP/APLPs is a crucial step in the pathology of Alzheimer disease and central to the physiological function of APP/APLPs.

For APP, a number of intracellular interaction partners, such as Fe65 (19), Fe65L1 (20), or X11α and X11β (21), are known to affect its processing. All of these proteins interact with the NPTY motif in the intracellular domain of APP, APLP1, and APLP2 via their phosphotyrosine binding (PTB) domain (22). Protein interacting with APP tail 1 (PAT1) binds to the basolateral sorting sequence (BaSS) of APP and is associated with microtubules. Further, an influence on APP cleavage at the cell surface has been proposed (23). Therefore, a kinesin light chain (KLC)-like function has been proposed (23). However, the structural and primary sequence homology between PAT1 and KLC is low. Additionally, PAT1 was shown not to interact with kinesin heavy chain (23), and its association to microtubules is elevated in the presence of ATP (23), indicating that PAT1 has no KLC-like function. It has also been reported that PAT1 affects the half-life time of the APP intracellular domain (AICD), suggesting a regulatory function of PAT1 in the putative nuclear signaling of the AICD (24). In this study, AICD fragments with a length of 57 (C57) and 59 (C59) amino acids were shown to be affected by PAT1. However, the majority of AICD released to the cytoplasm results from ϵ-cleavage, and it is not clear whether C57 and C59 are released to the cytosol *in vivo* (15, 25–29). Additionally, Ara67, which is 99.6% identical to PAT1, was reported as an androgen receptor-interacting protein, interrupting androgen receptor cytoplasmic-nuclear import and modulating androgen receptor signaling. These studies suggest that PAT1 might be a regulatory factor that

* This work was supported by grants from the Fritz-Thyssen Stiftung (to S. K.) and the Alzheimer Forschung Initiative e.V. (to S. K.). The costs of publication of this article were defrayed in part by the payment of page charges. This article must therefore be hereby marked "*advertisement*" in accordance with 18 U.S.C. Section 1734 solely to indicate this fact.

[S] The on-line version of this article (available at http://www.jbc.org) contains two supplemental figures.

[1] Both authors contributed equally to this work.

[2] Present address: Dept. of Physiology, University of California, San Francisco, San Francisco, CA 94143.

[3] Present address: Department of Neurosciences, University of California, San Diego, La Jolla, CA 92093.

[4] Present address: Cavalieri Ottolenghi Scientific Institute, 10123 Torino, Italy.

[5] To whom correspondence should be addressed: ZMBH, University of Heidelberg, Im Neuenheimer Feld 282, 69120 Heidelberg, Germany. Tel.: 49-6221-546847; Fax: 49-6221-545891; E-mail: s.kins@zmbh.uni-heidelberg.de.

[6] The abbreviations used are: Aβ, β-amyloid peptide; APP, β-amyloid precursor protein; sAPP, secreted APP; APLP, β-amyloid precursor-like protein; BaSS, basolateral sorting sequence; RNAi, RNA interference; BACE, β-site APP cleaving enzyme; CTF, C-terminal fragment; ICD, intracellular domain; AICD, APP intracellular domain; KLC, kinesin light chain; IB, immunoblotting; IC, immunocapture; HA, hemagglutinin; GST, glutathione *S*-transferase; ELISA, enzyme-linked immunosorbent assay; SNP, single nucleotide polymorphism; aa, amino acids; Tricine, *N*-[2-hydroxy-1,1-bis(hydroxymethyl)ethyl]glycine; sh, short hairpin; scr, scrambled.

controls the subcellular localization of multiple proteins with divergent functions.

Here we show that PAT1a, which is 99.0% identical to PAT1, exists in a common complex with APP, APLP1, and APLP2 *in vivo* and co-localizes with APP/APLPs bearing intracellular vesicles. Moreover, we demonstrate that PAT1a regulates the levels of APP family members at the cell surface. Finally, we provide evidence that PAT1a increases the proteolytic conversion of APP/APLPs and promotes the generation of Aβ, suggesting an important regulatory role of PAT1a in the transport of APP/APLPs with possible implications for Alzheimer disease pathogenesis.

EXPERIMENTAL PROCEDURES

Cloning of Human PAT1a—The PAT1a cDNA was amplified from a human brain cDNA library (Clontech) using open reading frame-flanking primers (sense, 5′-gaa gga aga tgg cgg ccg tgg-3′; antisense, 5′-cct cag cag ctc ggt ccc tcg aca ttc tg-3′) and cloned into the pCRII-TOPO vector (Invitrogen). For recombinant expression of PAT1a, the encoding cDNA was subcloned into pcDNA3.1 (Invitrogen). Alternatively, a hemagglutinin (HA) tag was fused to the 3′-end of the PAT1a cDNA by PCR and cloned into pcDNA3.1. For this purpose, the following oligonucleotides were used: sense, 5′-aat tgg tac cgc cgc cac cat ggc ggc cgt gga act aga gtg-3′, and antisense, 5′-gta att gcg gcc gct caa gcg tct tag ggg acg tcg tat ggg tag cag cac ggt ccc tcg aca ttc tg-3′.

Cell Fractionation and Carbonate Extraction—COS-7 or SH-SY5Y cells were co-transfected with PAT1a-HA and APP, APLP1, or APLP2 cDNAs. 28 h after transfection, cells were lysed in homogenization buffer (HOM) (250 mM sucrose, 5 mM HEPES, pH 7.4, 1 mM $MgCl_2$, 10 mM KCl, 1 mM phenylmethylsulfonyl fluoride) by passing 20 times through a 27-gauge needle and centrifuged at 100 × *g* for 5 min at 4 °C. The supernatant was added to a 9-fold higher volume of carbonate buffer (0.1 M Na_2CO_3, pH 11) and incubated for 15 min on ice. The postnuclear homogenate was then layered on a 1/3 volume of sucrose/carbonate buffer (carbonate buffer containing 0.25 M sucrose) and centrifuged at 100,000 × *g* for 45 min. Soluble proteins in the supernatant and membrane fractions in the pellet were analyzed by SDS-PAGE followed by Western blotting. The amounts of PAT1a associated with APP/APLPs in the membrane fraction or present in the fraction containing soluble proteins were quantified using Advanced Image Data Analyzer (AIDA) software, version 3.20.116 (Raytest Isotopen-Messgeräte GmbH).

GST Pulldown Analysis—The generation of GST fusion proteins containing the intracellular domain of APP (AICD, aa 649–695), APLP1 (ALICD1, aa 604–650), and APLP2 (ALICD2 aa 717–763) have been described previously (30). The cDNAs encoding ALICD1 and ALICD2 lacking the BaSS (aa 604–620 and aa 733–763) (ALICD1ΔBaSS and ALICD2ΔBaSS) were amplified by PCR and cloned by BamHI/NotI in-frame into pGEX4T-1 (Amersham Biosciences). The sequence was verified by sequencing of both strands (Agowa). Expression of GST and GST fusion proteins and loading of glutathione-Sepharose beads (Amersham Biosciences) was performed as described previously (31). PAT1a was *in vitro*-translated in the presence of [^{35}S]methionine (TnT7 quick-coupled transcription/translation system (Promega)) and incubated with the loaded beads in buffer H (50 mM Tris, pH 6.8, 50 mM KCl, 100 mM NaCl, 2 mM $CaCl_2$, 2 mM $MgCl_2$, 0,1% (w/v) Triton X-100, 5 mM dithiothreitol) for 90 min. After three times of washing with buffer H, the proteins were eluted and analyzed by 12% SDS-PAGE. Subsequently, gels were dried and subjected to autoradiography (MR films, Amersham Biosciences) overnight. Quantification is based on densitometric measurements using Image Gauge (Fuji Systems).

Antibodies—The monoclonal anti-HA and rat anti-c-Myc antibody were purchased from Roche Applied Science and the mouse anti-c-Myc (9E10) antibody was purchased from Santa Cruz Biotechnology. The β-tubulin antibody (mouse) was from Sigma. Monoclonal antibody against APP (22C11) has been described (32). The rabbit polyclonal antibodies against APLP1 (CT-11) and APLP2 (DII-2) were obtained from Calbiochem. For generation of an anti-PAT1a antibody, rabbits were immunized with synthesized peptide corresponding to the C-terminal residues 542–572 of human PAT1a. The resulting antiserum was affinity-purified using the same peptide (SulfoLink kit, Pierce). Primary antibodies were used at the following dilutions: anti-APP (22C11) 1:10,000 (IB); anti-PAT1a 1:500 (IB), 1:50 (IC); anti-APLP1 (CT11) 1:10,000 (IB); anti-APLP2 (D2-II) 1:10,000 (IB); anti-HA 1:2000 (IB), 1:200 (IC); anti c-Myc 1:200 (IC). For immunoblotting, secondary anti-rabbit and anti-mouse IgG antibodies (1:10,000) (Promega) and anti-rat IgG antibodies (1:10,000) (DAKO Diagnostic) conjugated to horseradish peroxidase were used. For immunofluorescence analysis, secondary anti-mouse, anti-rat, and anti-rabbit antibodies (1:500) were purchased from Molecular Probes (Alexa Fluor series).

Immunocytochemical Assays—For immunocytochemical analysis, primary neurons were fixed with 4% paraformaldehyde/phosphate-buffered saline for 10 min and permeabilized with 0.1% Nonidet P-40 in phosphate-buffered saline for 10 min. Staining of cells was performed using standard procedures (33, 34). The fluorescent signals were visualized with an Axiovert 200 M Inverted Microscope (Zeiss) supplied with a CCD Camera (Hamamatsu), and images were acquired and enhanced using the MetaMorph Imaging System (Universal Imaging Co.).

Cell Culture and Transfection—COS-7, HEK293, and SH-SY5Y cells were cultured under standard conditions. Primary neurons were prepared as described (35) with the exception that mouse cortical neurons of embryonic day 14 were used. Neurons were grown on poly-L-lysine-coated 15-mm coverslips (Marienfeld) in serum-free neurobasal medium (Invitrogen) with B-27 supplement (Invitrogen), 25 μM glutamate, and 0.5 mM glutamin. Cells were transfected with plasmid DNA using Lipofectamine Plus (Invitrogen) or Lipofectamine 2000 (Invitrogen) according to the manufacturer's instructions and collected for analysis 20–72 h after transfection.

Silencing of PAT1a Expression—For the down-regulation of PAT1a, a short hairpin (sh) construct (shPAT1a) was cloned into pSilencer1.0-U6 (Ambion) using the sequence previously described by Zhang *et al.* (36). A scrambled RNAi sequence directed against PAT1a (scrPAT1a) was cloned accordingly and served as a control. For cassette cloning of the shPAT1a con-

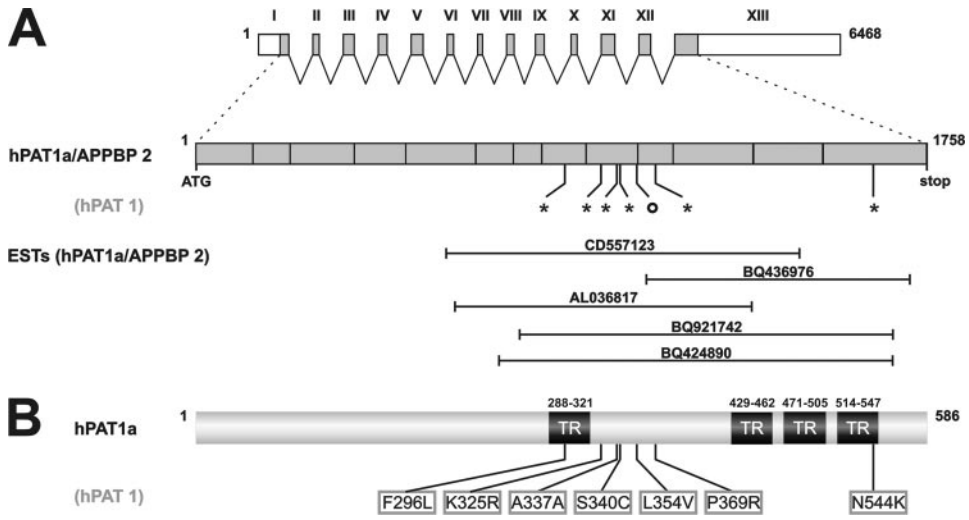

FIGURE 1. **Schematic representation of the genomic structure, cDNA, and protein organization of PAT1a/APPBP2 in comparison with PAT1.** *A*, the human PAT1a/APPBP2 (*hPAT1a/APPBP 2*) mRNA has a length of 6468 bp and is represented by 13 exons (*I–XIII*). Exon boundaries within the coding region of the PAT1a cDNA (1758 bp) are marked. The seven nucleotide exchanges present in the PAT1 sequence (*asterisk* and *open circle*), and the resulting mostly non-identical amino acid substitutions are indicated. Those nucleotide exchanges present in PAT1, which are annotated as SNPs in the genomic sequence, are marked by an *asterisk*. The accession numbers and relative positions of five expressed sequence tags that correspond to the PAT1a sequence are shown (see "Results" for details). *B*, protein structure of human PAT1a/APPBP2. The amino acid substitutions in the sequence of PAT1 in comparison with PAT1a/APPBP2 are indicated. The positions of predicted helix-loop-helix motifs with a significant homology to tetratricopeptide-like repeats (*TR*) are shown.

struct, the following two oligonucleotides were used: forward, 5′-cga agg cag aac agt taa ttt tca aga gaa att aac tgt tct gcc ttc ttt ttt g-3′, and reverse, 5′-aat tca aaa aag aag gca gaa cag tta att tct ctt gaa aat taa ctg ttc tgc ctt cgg gcc-3′. The non-functional scrPAT1a construct was generated by the same strategy, using the following oligonucleotides: forward, 5′-cga agg tag atc agc taa ttt tca aga gaa att aac tgt tct gcc ttc ttt ttt g-3′, and reverse, 5′-aat tca aaa aag aag gca gaa cag tta att tct ctt gaa aat tag ctg atc tac ctt cgg gcc-3′. The identity of the construct was confirmed by sequencing. SH-SY5Y cells were transfected with pSilencer sh-PAT1a and src-PAT1a using Lipofectamine 2000 (Invitrogen) according to the manufacturer's instructions and collected for analysis 48–72 h after transfection.

Co-Immunoprecipitation Assay—Adult mouse brains were homogenized in ice-cold co-immunoprecipitation buffer (10 mM HEPES, pH 7.2, 143 mM KCl, 5 mM $MgCl_2$, 1 mM EGTA, 1% Triton X-100, protease inhibitor mix (Roche Applied Science). Before immunoprecipitation, either anti-PAT1a antibody or preimmune serum as a control was incubated with protein A-Sepharose beads. Alternatively, antibodies were covalently coupled to an agarose gel (ProFundTM co-immunoprecipitation kit (Pierce)). For IPs, brain lysates of young adult mice (C57Bl/6) containing 400 μg of protein were incubated with beads loaded with anti-PAT1/PAT1a antibody or preimmune serum for 4 h at 4 °C. After extensive washing with co-immunoprecipitation buffer, immunocaptured protein samples were collected in sample buffer containing β-mercaptoethanol and analyzed by SDS-PAGE and Western blotting. The antigen/antibody-complexes were visualized using ECL detection (Amersham Biosciences).

Analyses of APP/APLPs Processing—SH-SY5Y cells were transfected as described previously. For the analysis of secreted sAPP/APLPs and Aβ, fresh growth medium was added to the cells after transfection (2.5 ml for each 6-cm dish and 1 ml for each well of a 6-well plate), conditioned for 30 h, and subsequently assayed for Aβ (ELISA) or analyzed by Western blotting. For the analysis of the full-length APP/APLPs and CTFs, cells were lysed 30 h after transfection for 30 min in ice-cold lysis buffer (50 mM Tris/HCl, pH 7.5, 150 mM NaCl, 1% Triton X-100, 5 mM EDTA, and Complete^{TM} protease inhibitor mixture (Roche Applied Science)) and centrifuged at 10,000 $\times$ *g*. The supernatants were denatured in sample buffer and analyzed by SDS-PAGE on 8% Tris-glycine or 15% Tris-Tricine gels and Western blotting.

Quantification of Aβ Using Sandwich ELISA Assay—Secreted Aβ levels were measured by a Sandwich ELISA assay (hAmyloid ELISA High Sensitive, The Genetics Company, Zürich, Switzerland) as described (37). Mouse monoclonal antibodies specific to Aβ40 (G2–10) or Aβ42 (G2–13) were used as capture antibodies, and an N-terminal Aβ antibody (W0–2) was used for detection. Aβ levels in the samples were determined by comparison with the signal from media spiked with known quantities of Aβ40 and Aβ42.

Surface Biotinylation—48 h after transfection with control plasmid, PAT1a cDNA, or shPAT1a, SH-SY5Y cells were washed with cold phosphate-buffered saline containing 0.2 mM $CaCl_2$ and 2 mM $MgCl_2$ followed by incubation with sulfo-NHS-LC-biotin (0.5 mg/ml, Pierce) for 1 h at 4 °C. The reaction was stopped by extensive washing with phosphate-buffered saline and quenched with 50 mM NH_4Cl, 1% bovine serum albumin in 50 mM Tris, pH 8.0. Cell lysates were prepared and precipitated with streptavidin-Sepharose (Amersham Biosciences). The precipitated biotinylated proteins were subjected to Western blot analysis. For detection of PAT1a or APP/APLPs, the indicated antibodies were used and visualized using horseradish peroxidase-conjugated secondary antibodies and enhanced chemiluminescence technique (Amersham Biosciences).

RESULTS

Polymorphism of the PAT1/APPBP2 Gene—As a prerequisite for our studies of the PAT1 protein, we amplified the coding region of PAT1 cDNA from a human brain cDNA library. Surprisingly, we consistently found seven nucleotide exchanges in eight independent clones, resulting in six amino acid substitutions (F296L, K325R, A337A, S340C, L354V, P369R, N544K) (Fig. 1). Data base analyses of the PAT1 sequence (cDNA, AF017782; aa, AAC83973.1) revealed that besides PAT1, a sequence (APPBP2 cDNA, NM_006380; aa, NP_006371.2) completely identical with the sequence we amplified from the

brain cDNA is annotated in the data base. Furthermore, we found that the genomic sequence, which is located on chromosome 17, is also identical to our brain cDNA PCR product and APPBP2 (LocusID: 10513). The Ensembl website gives no indication for a duplication of this gene in the human genome. We analyzed 53 expressed sequence tags covering the region of PAT1 cDNA containing the nucleotide exchanges and found that all tested expressed sequence tag sequences were identical with our brain cDNA PCR products and APPBP2, but none was equal to PAT1. These data indicate that the PAT1 sequence used in previous analyses (23, 24, 36) carries six amino acid exchanges. The PAT1 amino acid sequence is thus 99% identical to APPBP2. We conclude that the PAT1 sequence represents a rare variant of APPBP2 rather than a sequencing error as independently of the PAT1 sequence, six of seven nucleotide exchanges in the PAT1 sequence are annotated as single nucleotide polymorphisms (SNPs) in the genomic sequence. In addition, Ara67 has been described to be 99.6% identical with PAT1 (36), suggesting that *Ara67* is a further variant of *PAT1/APPBP2*. Thus, *PAT1*, *Ara67*, and *APPBP2* likely represent different alleles of one single gene, of which APPBP2 is the most common form. For simplification, we propose to rename APPBP2 to PAT1a.

Co-localization and Interaction of PAT1a with APP, APLP1, and APLP2 in Neurons—To test whether PAT1a interacts with APP and possibly also with APLP1 and APLP2 *in vivo*, we performed co-fractionation, co-immunoprecipitation, and co-localization experiments. In a cell fractionation assay, we found that about 50% of PAT1a co-fractionated with membranes containing APP/APLPs. Moreover, PAT1a can be released into the cytosolic fraction by carbonate extraction, showing that it is not a transmembrane protein nor coupled covalently to the membrane (data not shown). Together these data suggest that PAT1a is associated with membrane compartments containing APP, APLP1, and APLP2. To perform co-immunoprecipitation analysis, we generated a polyclonal anti-PAT1a antibody directed against an epitope in the C terminus of human PAT1a (amino acids 542–572). This region contains only one of the amino acid substitutions (N544K) when compared with PAT1/Ara67. Since we have not tested whether the antibody recognizes PAT1 and Ara67, we cannot exclude the possibility of cross-reactivity. However, we show that this anti-PAT1a antibody can be used for Western analyses and immunoprecipitation studies of recombinant HA-tagged PAT1a and endogenous PAT1a (possibly also PAT1 and Ara67) (Fig. 2 and see also Fig. 5). Co-immunoprecipitation experiments with mouse brain extracts using the anti-PAT1a antibody revealed that APP, APLP1, and APLP2 can be co-immunoprecipitated with PAT1a, suggesting that all three APP family members are interacting with PAT1a *in vivo* (Fig. 2). Co-immunoprecipitations with PAT1a preimmune serum served as control (Fig. 2). Noteworthily, the mature forms of APP, APLP1, and APLP2 were selectively co-immunoprecipitated with PAT1a, indicating specific interaction in post-Golgi compartments.

The specificity of the anti-APP, anti-APLP1, and anti-APLP2 antibodies was demonstrated in Western analyses of brain extracts from wild-type mice when compared with APP-, APLP1-, and APLP2-knock-out mice (supplemental

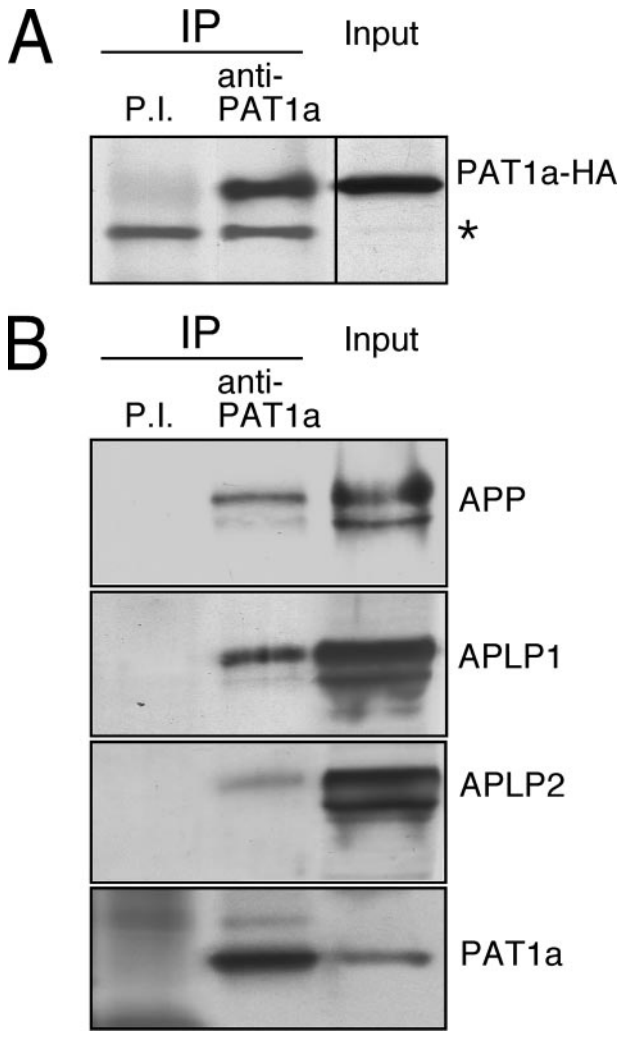

FIGURE 2. **Co-immunoprecipitation (*IP*) of PAT1a with APP, APLP1, and APLP2 from mouse brain extracts.** *A*, immunoprecipitation of recombinant PAT1a with the anti-PAT1a antibody in SH-SY5Y cells. Cell lysates of transiently transfected SH-SY5Y cells expressing HA-tagged PAT1a were incubated with anti-PAT1a antibody or preimmune serum (*P.I.*) as a control. The immunoprecipitates were detected in Western blot analysis with the anti-HA antibody. 20% of the cell homogenate (*Input*) was loaded as a control. In the lanes loaded with the immunoprecipitates besides PAT1a, the heavy chain of the IgG was detected (marked by an *asterisk*). *B*, in co-immunoprecipitation experiments from mouse brain extract, PAT1a was immunoprecipitated with the anti-PAT1a antibody. Samples lacking the PAT1a antibody (−) and samples with the corresponding preimmune serum served as controls. 1% of the brain homogenates (*Input*) were loaded as control. Western blot detection of APP, APLP1, and APLP2 was performed with the antibodies 22C11, CT11, and D2-II, respectively. PAT1a was detected with the anti-PAT1a antibody.

Fig. 1). We next investigated the cellular localization of PAT1a in mixed cortical neurons. Since we so far could not establish conditions that allow immunocytochemical analyses of endogenous PAT1a, we transfected primary neurons differentiated for 7 days *in vitro* with a cDNA encoding HA-tagged PAT1a. We observed a diffuse cytosolic staining as well as punctuate vesicular PAT1a immunoreactivity, suggesting that PAT1a is partly associated with intracellular vesicles (Fig. 3). We also detected a strong PAT1a immunoreactivity in the somatodendritic compartment and in MAP2-negative neurites, indicating that PAT1a is localized to both dendrites and axons (data not shown). In non-neuronal cells, a

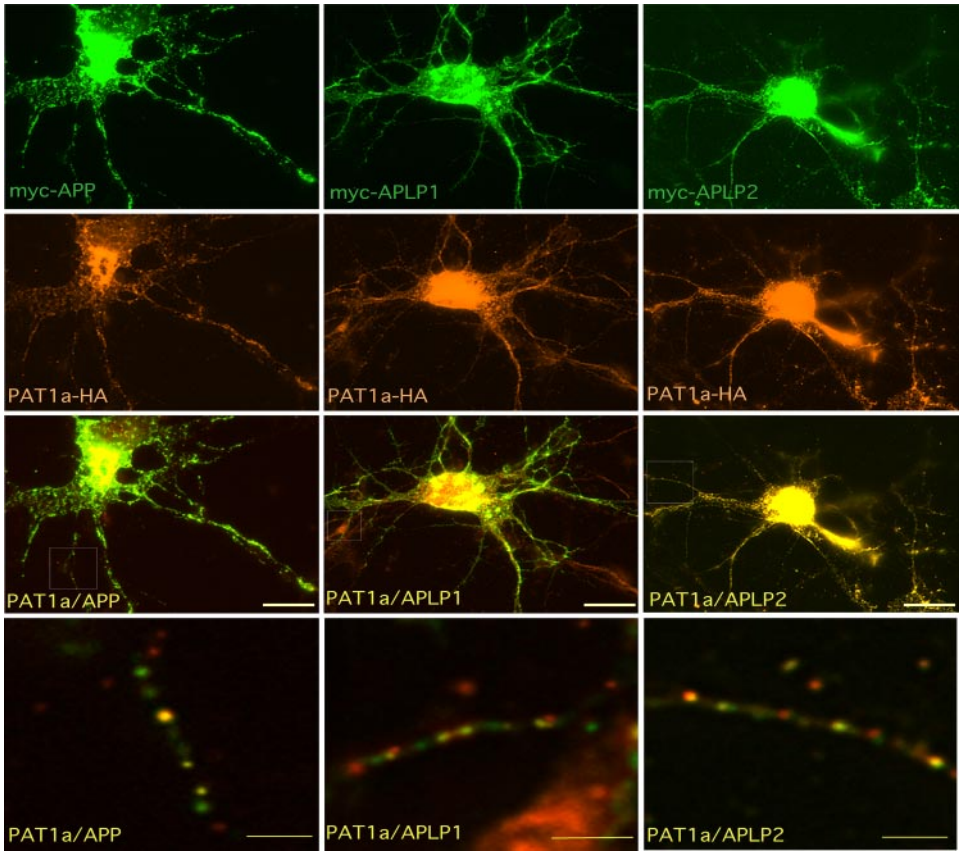

FIGURE 3. **PAT1a is associated with APP-, APLP1-, and APLP2-containing vesicles.** Mixed cortical neurons (mouse, embryonic day 14) were transfected with cDNAs encoding HA-tagged PAT1a and Myc-tagged APP, APLP1, or APLP2. Cells were stained with the anti-PAT1a (*red*) and anti-Myc (*green*) antibodies. These co-stainings revealed co-localization of APP-, APLP1-, and APLP2-positive vesicular components with PAT1a immuoreactivity (*yellow*). The *lower three images* show a higher magnification of the area marked in the merged images by a *square*. Note that the highest degree of co-localization was observed for PAT1a and APLP2. Bar, *upper panels*, 10 μm; *lower three panels*, 2 μm.

mixed nuclear and cytosolic localization of PAT1 was reported (24), which could be confirmed in our studies using neuronal (SH-SY5Y, N2a, primary cortical neurons) and non-neuronal cells (COS-7 and HEK293) (supplemental Fig. 2). Finally, we investigated whether PAT1a co-localizes with APP, APLP1, or APLP2. For this purpose, primary neurons were transfected with cDNAs encoding HA-tagged PAT1a and Myc-tagged APP, APLP1, or APLP2. Immunocytochemical analysis revealed co-localization of PAT1a with APP, APLP1, or APLP2 in vesicular structures of distal neurites (Fig. 3). Remarkably, not all APP/APLP-positive vesicles were co-stained with PAT1a. This suggests that PAT1a is associated with a specific subset of APP/APLP-containing vesicles in the early and late secretory pathway or in endosomes. Taken together, these data show that PAT1a is associated with vesicular membranes containing APP/APLPs, suggesting a function of PAT1a in APP/APLPs trafficking.

PAT1a Binds Directly to the BaSS of APP, APLP1, and with the Highest Affinity to APLP2—To investigate whether the association of PAT1a with APP-, APLP1-, and APLP2-containing vesicles is mediated via a direct binding of PAT1a to the intracellular domain of APP/APLPs, we performed GST pulldown experiments with *in vitro*-translated PAT1a and GST fused to the intracellular domain of APP (AICD), APLP1 (ALICD1), and APLP2 (ALICD2), respectively. We found that PAT1a was specifically retained on beads loaded with GST-AICD but did not bind to beads loaded with GST alone (Fig. 4). However, the binding capacity of PAT1a to AICD was low (only 2-fold above background), which is consistent with previous studies (23). The APLP1 and APLP2 intracellular domains also bound PAT1a. Interestingly, ALICD2 showed stronger binding to PAT1a than ALICD1 or AICD (10-fold above background) (Fig. 4). Kinesin light chain 1 (KLC1), which has a similar structure as PAT1a, did not bind to GST-AICD, -ALICD1, or -ALICD2 fusion proteins under the same conditions, demonstrating the specificity of our GST pulldown analysis (30). Deletion mapping experiments, based on two-hybrid analysis and GST pulldown studies of APP and PAT1, have previously shown that PAT1 binds to the BaSS of APP (23). To investigate the role of the BaSS in PAT1a binding to APLP1 and APLP2, we generated a mutant GST-ALICD1 and GST-ALICD2 lacking the BaSS (GST-ALICD1ΔBaSS and GST-ALICD2ΔBaSS). Neither GST-ALICD1ΔBaSS nor GST-ALICD-2ΔBaSS were interacting with PAT1a, demonstrating a direct binding of PAT1a to the BaSS of APP, APLP1, and APLP2.

PAT1a Facilitates the Trafficking of APP, APLP1, and APLP2 to the Cell Surface—To test whether PAT1a plays a role in the regulation of subcellular transport of APP/APLPs, we examined the influence of PAT1a expression on APP/APLP trafficking to the cell surface. For this purpose, we generated a short hairpin construct to mediate a knockdown of PAT1a (shPAT1a). A non-functional RNAi construct (scrPAT1a) served as a control.

Endogenous PAT1a levels were determined with our anti-PAT1a antibody. PAT1a was detected in Western blot analyses of cell lysates from SH-SY5Y cells overexpressing HA-tagged PAT1a and in cell lysates of non-transfected SH-SY5Y at 67 kDa, corresponding to the calculated molecular mass (66.9 kDa) (Fig. 5*A*). Under PAGE conditions optimized for separation of proteins with a molecular mass between 60 and 80 kDa, two forms of PAT1a could be differentiated (Fig. 5*B*). The difference in the apparent molecular weight might be explained by different phosphorylation states of PAT1a or other post-translational modifications. An anti-HA antibody recognized proteins with the same molecular weight in PAT1a-HA expressing cells but not in control cells transfected with empty vector. The overexpression rate of PAT1a was about 3–5-fold higher than

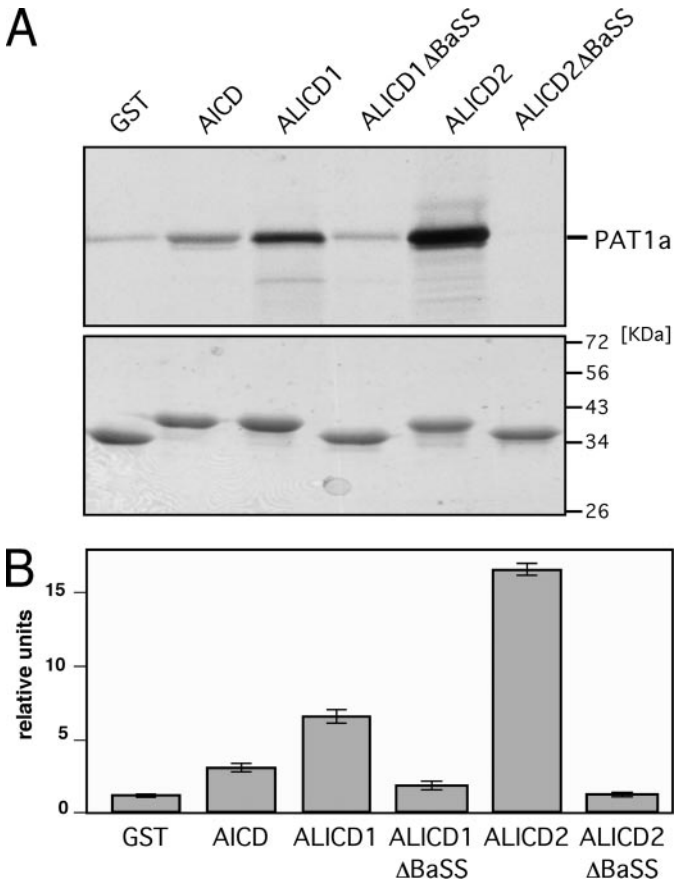

FIGURE 4. **Direct interaction of PAT1a with the intracellular domain of APP, APLP1, and APLP2.** Glutathione-Sepharose beads were loaded with GST fused to the intracellular domains (*ID*) of APP (*AICD*), APLP1 (*ALICD1*), APLP2 (*ALICD2*), or ALICD1 and ALICD2 lacking the basolateral sorting signal (*ALICD1ΔBaSS*, *ALICD2ΔBaSS*). Beads loaded with GST alone served as a negative control. *A*, autoradiography of radioactively labeled PAT1a (*upper panel*). Beads loaded with GST-AICD, -ALICD1, or -ALICD2, but not GST alone or GST-ALICD1ΔBaSS and GST-ALICD2ΔBaSS, bound to *in vitro*-translated PAT1a. To show equal loading of the beads, the GST fusion proteins were eluted from the beads, separated by PAGE, and stained with Coomassie Blue (*lower panel*). *C*, the results of at least three independent experiments were quantified by densitometric measurements and normalized to the signal obtained from GST beads. The mean ± S.E. is indicated.

endogenous PAT1a protein levels. Additionally, both antibodies, the anti-PAT1a and the anti-HA antibody, recognized lower molecular weight bands after longer exposure times, which may represent C-terminal cleavage products of PAT1a (data not shown). PAT1a RNAi treatment of COS-7 and SH-SY5Y cells reduced PAT1a levels to 30–50%, whereas β-tubulin protein levels were not affected (Fig. 5*B* and data not shown).

To evaluate whether PAT1a influences surface trafficking of APP/APLPs, we compared the amounts of surface APP, APLP1, and APLP2 in the presence of increased or reduced expression levels of PAT1a by cell surface biotinylation studies. Cells overexpressing PAT1a showed increased levels of surface APP and APLP2, whereas the PAT1a knockdown caused a reduction of APP and APLP2 at the plasma membrane. Altered PAT1a expression affected the APLP1 surface expression in a similar way, but in contrast to the influence on APP and APLP2, not significantly. However, manipulating PAT1a expression had no effect on total levels of APP, APLP1, and APLP2, suggesting a PAT1a-dependent relocalization of APP/APLPs to the cell surface.

PAT1a Affects Processing of APP, APLP1, and APLP2—Assuming that PAT1a regulates the anterograde transport of APP/APLPs to the cell surface, it should consequently affect the proteolytic conversion of APP/APLPs. Besides the Golgi apparatus, the plasma membrane is one of the two major sites where α-secretase cleavage of APP takes place (9, 38). In contrast, BACE 1 is most active at mildly acidic pH (11), making endosomes the most likely location for BACE cleavage of APP. Moreover, BACE 1 was reported to be cycling between the cell surface and endosomes (39). It was also shown that internalization of cell surface APP via endocytosis leads to elevated Aβ generation and release into the medium (40). To test the impact of elevated or reduced levels of PAT1a on processing of APP/APLPs, we used SH-SY5Y and COS-7 cells expressing APP, APLP1, or APLP2 fused to a tandem z-domain (2z), which was used as it facilitates the detection of all APP/APLP CTFs (8, 15). The cells were additionally co-transfected with HA-tagged PAT1a, the PAT1a RNAi construct, or a non-functional RNAi construct (srcPAT1a) as a control. Cells coexpressing PAT1a showed elevated levels of sAPP, sAPLP1, and sAPLP2, as well as increased amounts of the corresponding CTFs. On the other hand, the reduction of PAT1a expression led to decreased secretion of sAPP/sAPLPs and lower CTF levels (Fig. 5). Remarkably, PAT1a affected α-, β-, and γ-CTF generation to a very similar extent (Fig. 6), which argues in favor of a function in anterograde transport of APP/APLPs.

Influence of PAT1a on the Generation of Aβ40/42—Since PAT1a influenced APP/APLPs CTF generation, we assumed that PAT1a should also affect Aβ production. To test this assumption, we collected conditioned medium of human neuroblastoma cells (SH-SY5Y) expressing APP, APLP1, or APLP2 fused to a 2z-domain and different levels of PAT1a (as a consequence of transfection with PAT1a cDNA, scrPAT1a, or shPAT1a) 48 h after transfection. Aβ40 and Aβ42 levels were determined using ELISA measurements. Consistent with the observed effect of PAT1a on β-CTF and ϵ-CTFs generation, we found that cells overexpressing PAT1a generated elevated levels of Aβ, whereas cells with reduced levels of PAT1a produced less Aβ. No difference in the ratio of Aβ40 to Aβ42 was observed. These data demonstrate that altered PAT1a expression affects Aβ production, suggesting a regulatory role in the pathogenesis of Alzheimer disease.

DISCUSSION

In this study, we show that PAT1a binds to all APP family members *in vivo* and associates with APP-, APLP1-, and APLP2-containing vesicles in neurons, likely through direct interaction with their ICDs. We also demonstrate that PAT1a regulates the cell surface levels of APP/APLPs. Moreover, we show that PAT1a promotes the cleavage of APP/APLPs by α-, β-, and γ-secretases, resulting in elevated secretion of sAPP/sAPLPs, increased production of α-, β-, and ϵ-cleaved CTFs, and elevated levels of Aβ.

Our data base and PCR analyses of brain cDNA revealed that the sequence differences in PAT1 and Ara67 are due to SNPs in the *PAT1a/APPBP2* gene, indicating a high variance in this

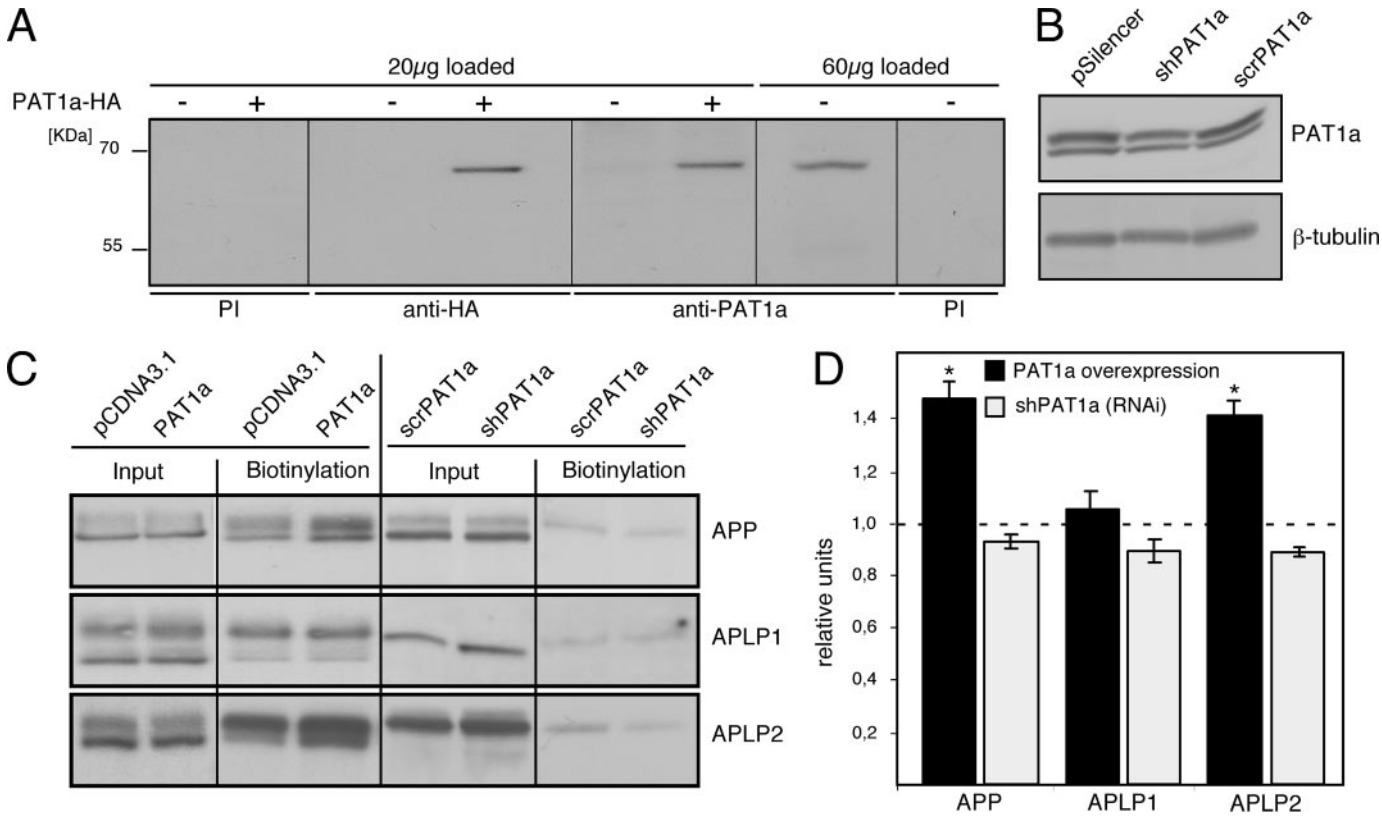

FIGURE 5. **Cell surface localization of APP depends on PAT1a expression.** *A*, to determine the endogenous PAT1a protein levels, an anti-PAT1a antibody was generated. Depending on the gel system and degree of separation, it recognizes a very close double band (*B*) at ~67 kDa in protein extracts (20 μg) of SH-SY5Y cells expressing recombinant PAT1a tagged with a HA tag (*PAT1a-HA*). The difference in the apparent molecular weight may be due to different post-translational modifications of PAT1a, such as phosphorylation. On the blot in *panel A*, the proteins were less well separated when compared with the blot in *panel B*. Thus, PAT1a appears as a single band or as a double band, respectively. Probing of the same extract with a HA antibody revealed an identical signal. After loading of higher amounts of protein extracts (60 μg), the anti-PAT1a antibody also detected endogenous PAT1a in non-transfected cells with the same apparent molecular weight. The overexpression rate of PAT1a was about 3–5-fold higher than endogenous PAT1a protein levels. *B*, SH-SY5Y cells were treated with transfection reagent only, with shPAT1a, or with a non-functional RNAi construct (*scrPAT1a*). 48 h after transfection, cell lysates were analyzed on a 8% Tris-glycine gel and subjected to Western analysis using anti-PAT1a and anti-β-tubulin antibodies. *C*, biotinylation assay 48 h after transfection with PAT1a cDNA, for control pCDNA3.1 or shPAT1a, and for control scrPAT1a. Cells were incubated at 4 °C for 1 h with a biotinylation reagent. Cell extracts were prepared, and biotinylated surface proteins were immunoprecipitated. Western analysis was performed with anti-APP, anti-APLP1, or anti-APLP2 antibodies. *D*, for quantification, densitometric measurements of three independent experiments were performed. The data were normalized to the amount of total APP, APLP1, and APLP2. The mean ± S.E. is indicated. Statistically significant differences in comparison with control cells transfected with pCDNA3.1 (served as control for PAT1a overexpression) or the scrPAT1a construct (served as control for PAT1a knockdown) (Mann-Whitney U-test) with a p value <0.05 are marked by an *asterisk*.

gene. Detailed investigations will be necessary to determine the precise frequency of SNPs and whether these nucleotide exchanges have an impact on the binding affinity of PAT1a to APP/APLPs, which could affect APP processing.

PAT1a was reported to be a nucleocytoplasmic protein, but so far, only cytosolic functions of PAT1a/Ara67 have been proposed (23, 24, 36). However, we also observed nuclear localization of PAT1a in non-neuronal cell lines,[7] but we did not find any specific PAT1a immunoreactivity in the nuclei of primary neurons, although PAT1a was expressed at high levels. Therefore, a nuclear function of PAT1a in neurons appears unlikely. However, we found that in primary neurons, PAT1a co-fractionates and co-localizes with membrane compartments containing APP/APLPs. Although we did not determine the specific character of these vesicles, their morphology and localization in distal neurites suggests that they are vesicular components of the secretory or endocytotic pathway. Thus, under consideration of our studies showing an influence of PAT1a on the amount of APP/APLPs at the cell surface, we propose that PAT1a either facilitates the transport of APP/APLPs to the cell surface or inhibits their endocytosis rate. Consistently, we found that PAT1a binds directly to the juxtamembrane region of the intracellular domain of APP/APLPs. The BaSS has previously been shown to be important for transport of APP to the cell surface, APP internalization, and basolateral transport of APP and APLP2 in MDCK cells (41–43).

All APP family members are predominantly cleaved in the late secretory pathway, including the plasma membrane and endosomes (44). We found that PAT1a affects APP/APLPs processing in a way that simultaneously increases or decreases α-, β-, and γ-cleavage depending on increased or decreased expression of PAT1a, respectively. Since all processing steps including ϵ-CTF and Aβ production were similarly affected, it might be possible that PAT1a regulates α-, β-, and γ-secretase activities. However, this is unlikely as activation of the involved proteases relies on different molecular mechanisms. Interestingly, several adaptor proteins are known to influence APP transport and processing. Fe65 overexpression was shown to

[7] Y.-H. Kuan and S. Kins, unpublished observation.

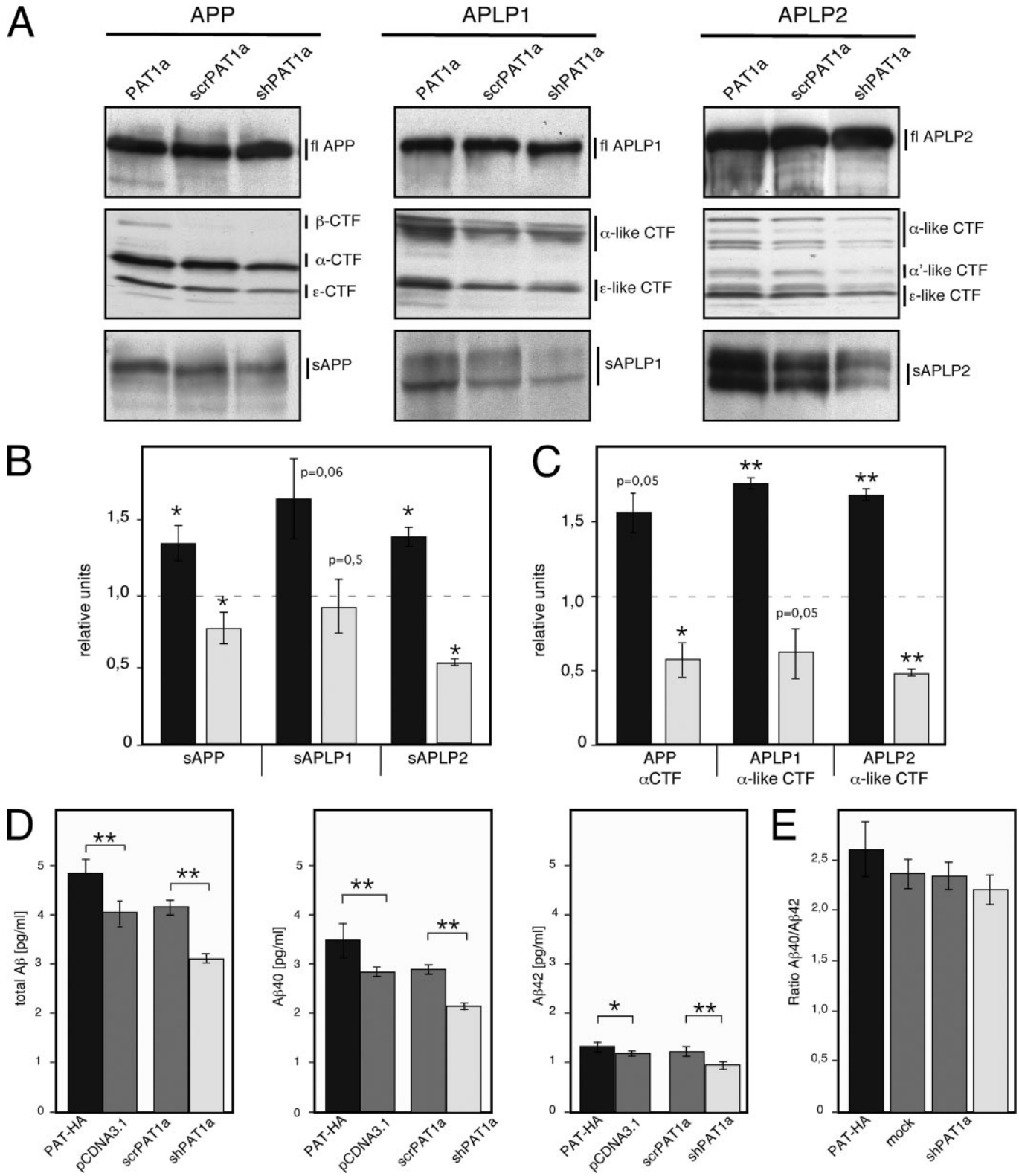

FIGURE 6. **PAT1a affects APP/APLP processing.** The influence of PAT1a on APP/APLP processing was analyzed in SH-SY5Y cells co-transfected with APP-, APLP1-, or APLP2-2z plasmids and PAT1a cDNA (b*lack column*), pCNA3.1 (empty vector, *gray column*), srcPAT1a (non-functional RNAi construct, *gray column*), or shPAT1a (RNAi, *black column*). *A*, after 48 h, medium containing sAPP, sAPLP1, or sAPLP2, and the cell extracts containing full length (*fl*) and CTFs of APP, APLP1, and APLP2 were subjected to Western analyses. *B* and *C*, the amounts of sAPP/APLPs (*B*) and α-/α-like CTFs (*C*) generated in cells with different PAT1a expression levels were quantified. The relative amounts of CTFs and secreted fragments in comparison with srcPAT1a or pCDNA3.1-transfected cells (indicated by *pCDNA3.1* (served as control for PAT1a overexpression) or the scrPAT1a construct (served as control for PAT1a knockdown) were set to 1) are shown. APP/APLPs full-length protein levels varied in the range of less than ± 5%. *Error bars* show S.E. ($n \geq 3$). *D*, 48 h after co-transfection of SH-SY5Y cells with APP-2z and PAT1a cDNA, pCDNA3.1, scrPAT1a, or shPAT1a, the conditioned medium was subjected to ELISA analysis to determine Aβ40 and Aβ42 levels. *Error bars* show standard deviations of the mean ($n \geq 3$). Statistical significant differences (Mann-Whitney U-test) with a p value <0.05 and <0.01 are marked by a *single asterisk* or *two asterisks*, respectively. *E*, determination of the ratio of Aβ40/Aβ42.

enhance APP secretion (19, 45). In contrast, X11α overexpression blocks APP maturation and secretion (21, 46), whereas the knockdown of X11α increases APP α- and β-CTFs but decreases Aβ levels (47).

As described in this work, the observed concomitant increase or decrease in all processing steps strongly suggests that PAT1a is a limiting factor to deliver APP/APLPs to compartments with secretase activity. In light of the distinct subcellular localization of the different secretase activities, namely the plasma membrane for α-secretase (9, 38) and endocytic compartments for β/γ-secretases (11, 39, 48–50), a function of PAT1a in APP/APLPs transport to the cell surface appears most likely. This view is further corroborated by the regulatory effect of PAT1a on cell surface levels of APP/APLPs. Although controversial, inhibition of endocytosis using a dynamin mutant was reported to retain elevated levels of APP at the cell surface, leading to increased α-cleavage. Surprisingly, β-secretase cleavage and Aβ production were enhanced as well (51, 52). Therefore, we cannot exclude that PAT1a may also reduce the endocytosis rate of APP/APLPs.

Further, the manipulation of PAT1a expression had different effects on processing and cell surface levels of APP/APLPs. For example, APLP1 processing was clearly affected by altered PAT1a expression, whereas the cell surface levels of APLP1 were not significantly changed. This indicates that PAT1a might affect the intracellular transport of APP/APLPs by increasing the proportion of APP/APLPs in compartments with active α- and β-secretases, which does not necessarily lead to a pronounced accumulation of the full-length APP/APLPs at the cell surface.

In conclusion, we hypothesize that PAT1a is controlling the intracellular localization of APP/APLPs, and by these means, also the proteolytic cleavage of all APP family members.

Acknowledgments—We thank I. Tomic and A. Trutzel for excellent technical assistance, G. Multhaup for help in antibody generation, J. A. Tschäpe and T. Hartmann for help performing ELISA measurements, and L. Ringrose for helpful suggestions for the manuscript.

REFERENCES

1. Kang, J., Lemaire, H. G., Unterbeck, A., Salbaum, J. M., Masters, C. L., Grzeschik, K. H., Multhaup, G., Beyreuther, K., and Muller-Hill, B. (1987) *Nature* **325,** 733–736
2. Wasco, W., Bupp, K., Magendantz, M., Gusella, J. F., Tanzi, R. E., and Solomon, F. (1992) *Proc. Natl. Acad. Sci. U. S. A.* **89,** 10758–10762
3. Paliga, K., Peraus, G., Kreger, S., Durrwang, U., Hesse, L., Multhaup, G., Masters, C. L., Beyreuther, K., and Weidemann, A. (1997) *Eur. J. Biochem.* **250,** 354–363
4. Wasco, W., Gurubhagavatula, S., Paradis, M. D., Romano, D. M., Sisodia, S. S., Hyman, B. T., Neve, R. L., and Tanzi, R. E. (1993) *Nat. Genet.* **5,** 95–100
5. Sprecher, C. A., Grant, F. J., Grimm, G., O'Hara, P. J., Norris, F., Norris, K., and Foster, D. C. (1993) *Biochemistry* **32,** 4481–4486
6. Coulson, E. J., Paliga, K., Beyreuther, K., and Masters, C. L. (2000) *Neurochem. Int.* **36,** 175–184
7. Soba, P., Eggert, S., Wagner, K., Zentgraf, H., Siehl, K., Kreger, S., Lower, A., Langer, A., Merdes, G., Paro, R., Masters, C. L., Muller, U., Kins, S., and Beyreuther, K. (2005) *EMBO J.* **24,** 3624–3634
8. Eggert, S., Paliga, K., Soba, P., Evin, G., Masters, C. L., Weidemann, A., and Beyreuther, K. (2004) *J. Biol. Chem.* **279,** 18146–18156
9. Lammich, S., Kojro, E., Postina, R., Gilbert, S., Pfeiffer, R., Jasionowski, M., Haass, C., and Fahrenholz, F. (1999) *Proc. Natl. Acad. Sci. U. S. A.* **96,** 3922–3927
10. Buxbaum, J. D., Liu, K. N., Luo, Y., Slack, J. L., Stocking, K. L., Peschon, J. J., Johnson, R. S., Castner, B. J., Cerretti, D. P., and Black, R. A. (1998) *J. Biol. Chem.* **273,** 27765–27767
11. Vassar, R., Bennett, B. D., Babu-Khan, S., Kahn, S., Mendiaz, E. A., Denis, P., Teplow, D. B., Ross, S., Amarante, P., Loeloff, R., Luo, Y., Fisher, S., Fuller, J., Edenson, S., Lile, J., Jarosinski, M. A., Biere, A. L., Curran, E., Burgess, T., Louis, J. C., Collins, F., Treanor, J., Rogers, G., and Citron, M. (1999) *Science* **286,** 735–741
12. Li, Q., and Sudhof, T. C. (2004) *J. Biol. Chem.* **279,** 10542–10550
13. Takasugi, N., Tomita, T., Hayashi, I., Tsuruoka, M., Niimura, M., Takahashi, Y., Thinakaran, G., and Iwatsubo, T. (2003) *Nature* **422,** 438–441
14. Edbauer, D., Winkler, E., Regula, J. T., Pesold, B., Steiner, H., and Haass, C. (2003) *Nat. Cell Biol.* **5,** 486–488
15. Weidemann, A., Eggert, S., Reinhard, F. B., Vogel, M., Paliga, K., Baier, G., Masters, C. L., Beyreuther, K., and Evin, G. (2002) *Biochemistry* **41,** 2825–2835
16. Walsh, D. M., Fadeeva, J. V., LaVoie, M. J., Paliga, K., Eggert, S., Kimberly, W. T., Wasco, W., and Selkoe, D. J. (2003) *Biochemistry* **42,** 6664–6673
17. Scheinfeld, M. H., Matsuda, S., and D'Adamio, L. (2003) *Proc. Natl. Acad. Sci. U. S. A.* **100,** 1729–1734
18. Cao, X., and Sudhof, T. C. (2001) *Science* **293,** 115–120
19. Sabo, S. L., Lanier, L. M., Ikin, A. F., Khorkova, O., Sahasrabudhe, S., Greengard, P., and Buxbaum, J. D. (1999) *J. Biol. Chem.* **274,** 7952–7957
20. Chang, Y., Tesco, G., Jeong, W. J., Lindsley, L., Eckman, E. A., Eckman, C. B., Tanzi, R. E., and Guenette, S. Y. (2003) *J. Biol. Chem.* **278,** 51100–51107
21. Sastre, M., Turner, R. S., and Levy, E. (1998) *J. Biol. Chem.* **273,** 22351–22357
22. King, G. D., and Scott Turner, R. (2004) *Exp. Neurol.* **185,** 208–219
23. Zheng, P., Eastman, J., Vande Pol, S., and Pimplikar, S. W. (1998) *Proc. Natl. Acad. Sci. U. S. A.* **95,** 14745–14750
24. Gao, Y., and Pimplikar, S. W. (2001) *Proc. Natl. Acad. Sci. U. S. A.* **98,** 14979–14984
25. Gu, Y., Misonou, H., Sato, T., Dohmae, N., Takio, K., and Ihara, Y. (2001) *J. Biol. Chem.* **276,** 35235–35238
26. Sastre, M., Steiner, H., Fuchs, K., Capell, A., Multhaup, G., Condron, M. M., Teplow, D. B., and Haass, C. (2001) *EMBO Rep.* **2,** 835–841
27. Yu, C., Kim, S. H., Ikeuchi, T., Xu, H., Gasparini, L., Wang, R., and Sisodia, S. S. (2001) *J. Biol. Chem.* **276,** 43756–43760
28. Zhao, G., Cui, M. Z., Mao, G., Dong, Y., Tan, J., Sun, L., and Xu, X. (2005) *J. Biol. Chem.* **280,** 37689–37697
29. Zhao, G., Mao, G., Tan, J., Dong, Y., Cui, M. Z., Kim, S. H., and Xu, X. (2004) *J. Biol. Chem.* **279,** 50647–50650
30. Lazarov, O., Morfini, G. A., Lee, E. B., Farah, M. H., Szodorai, A., DeBoer, S. R., Koliatsos, V. E., Kins, S., Lee, V. M., Wong, P. C., Price, D. L., Brady, S. T., and Sisodia, S. S. (2005) *J. Neurosci.* **25,** 2386–2395
31. Fuhrmann, J. C., Kins, S., Rostaing, P., El Far, O., Kirsch, A., Sheng, M., Triller, A., Betz, H., and Kneussel, M. (2002) *J. Neurosci.* **22,** 5393–5402
32. Hilbich, C., Monning, U., Grund, C., Masters, C. L., and Beyreuther, K. (1993) *J. Biol. Chem.* **268,** 26571–26577
33. Kins, S., Kurosinski, P., Nitsch, R. M., and Gotz, J. (2003) *Am. J. Pathol.* **163,** 833–843
34. Kins, S., Betz, H., and Kirsch, J. (2000) *Nat. Neurosci.* **3,** 22–29
35. Tienari, P. J., Ida, N., Ikonen, E., Simons, M., Weidemann, A., Multhaup, G., Masters, C. L., Dotti, C. G., and Beyreuther, K. (1997) *Proc. Natl. Acad. Sci. U. S. A.* **94,** 4125–4130
36. Zhang, Y., Yang, Y., Yeh, S., and Chang, C. (2004) *Mol. Cell. Biol.* **24,** 1044–1057
37. Duering, M., Grimm, M. O., Grimm, H. S., Schroder, J., and Hartmann, T. (2005) *Neurobiol. Aging* **26,** 785–788
38. Skovronsky, D. M., Moore, D. B., Milla, M. E., Doms, R. W., and Lee, V. M. (2000) *J. Biol. Chem.* **275,** 2568–2575
39. Huse, J. T., Pijak, D. S., Leslie, G. J., Lee, V. M., and Doms, R. W. (2000) *J. Biol. Chem.* **275,** 33729–33737

40. Koo, E. H., and Squazzo, S. L. (1994) *J. Biol. Chem.* **269,** 17386–17389
41. Haass, C., Koo, E. H., Teplow, D. B., and Selkoe, D. J. (1994) *Proc. Natl. Acad. Sci. U. S. A.* **91,** 1564–1568
42. Lo, A. C., Thinakaran, G., Slunt, H. H., and Sisodia, S. S. (1995) *J. Biol. Chem.* **270,** 12641–12645
43. Lai, A., Gibson, A., Hopkins, C. R., and Trowbridge, I. S. (1998) *J. Biol. Chem.* **273,** 3732–3739
44. Yamazaki, T., Koo, E. H., and Selkoe, D. J. (1996) *J. Cell Sci.* **109,** 999–1008
45. Santiard-Baron, D., Langui, D., Delehedde, M., Delatour, B., Schombert, B., Touchet, N., Tremp, G., Paul, M. F., Blanchard, V., Sergeant, N., Delacourte, A., Duyckaerts, C., Pradier, L., and Mercken, L. (2005) *J. Neurochem.* **93,** 330–338
46. Borg, J. P., Yang, Y., De Taddeo-Borg, M., Margolis, B., and Turner, R. S. (1998) *J. Biol. Chem.* **273,** 14761–14766
47. Xie, Z., Romano, D. M., and Tanzi, R. E. (2005) *J. Biol. Chem.* **280,** 15413–15421
48. Cupers, P., Bentahir, M., Craessaerts, K., Orlans, I., Vanderstichele, H., Saftig, P., De Strooper, B., and Annaert, W. (2001) *J. Cell Biol.* **154,** 731–740
49. Kaether, C., Lammich, S., Edbauer, D., Ertl, M., Rietdorf, J., Capell, A., Steiner, H., and Haass, C. (2002) *J. Cell Biol.* **158,** 551–561
50. Ray, W. J., Yao, M., Mumm, J., Schroeter, E. H., Saftig, P., Wolfe, M., Selkoe, D. J., Kopan, R., and Goate, A. M. (1999) *J. Biol. Chem.* **274,** 36801–36807
51. Chyung, J. H., and Selkoe, D. J. (2003) *J. Biol. Chem.* **278,** 51035–51043
52. Ehehalt, R., Keller, P., Haass, C., Thiele, C., and Simons, K. (2003) *J. Cell Biol.* **160,** 113–123